2A.4

THE NCEP NORTH AMERICAN MESOSCALE MODELING SYSTEM: RECENT CHANGES AND FUTURE PLANS

Eric Rogers*, Geoffrey DiMego, Thomas Black, Michael Ek, Brad Ferrier, George Gayno, Zavisa Janjic, Ying Lin, Matthew Pyle, Vince Wong, and Wan-Shu Wu
NOAA/NWS/NCEP/EMC, Camp Springs, Maryland

Jacob Carley
Purdue University, West Lafayette, Indiana

1. INTRODUCTION

In June 2006, NCEP implemented into the North American Mesoscale (NAM) modeling system and the NAM Data Assimilation System (NDAS) the Weather Research and Forecast version of the Non-Hydrostatic Mesoscale Model (WRF-NMM, Janjic, 2003, 2005) and the regional NCEP Grid-Point Statistical Interpolation (GSI) analysis (Wu *et al*., 2002). These replaced the Eta Model and the Eta 3DVAR analysis. See Rogers *et al*. (2005) for a description of the significant differences between the Eta Model and the WRF-NMM.

In December 2006 numerous changes were implemented to the WRF-NMM's convective parameterization and cloud microphysics. Additional changes were made to increase divergence damping to reduce model noise. Space limitations prevent an overview of these changes in this paper, but details can be found online at http://www.emc.ncep.noaa.gov/mmb/namchanges_dec2006/nam_upgrades.nov2006.html .

During 2008 two upgrades to the NDAS/NAM system were implemented which led to significant improvement in the skill of NAM forecasts as measured by quantitative scores. The motivation for these changes was to address poor NDAS/NAM performance (as reported by public and private sector forecasters) and known deficiencies in the system. This paper will discuss the components of both 2008 NAM upgrades, selected examples, and the overall impact of the full set of changes on NAM forecast performance. A brief description of future changes to the NDAS/NAM will be given in the concluding remarks.

2. 31 MARCH 2008 CHANGES

A description of each component of the March 2008 NAM change package and their impact on analyses and forecasts can be found online at http://www.emc.ncep.noaa.gov/mmb/namchanges_winter2008/nam_upgrades.2008.html .

* *Corresponding author address:* Eric Rogers, NOAA/NWS, 5200 Auth Road, Camp Springs, MD 20746-4304; e-mail: eric.rogers@noaa.gov

2.1 *Expanded Computational Domain*

Fig.1 shows the enlarged computational domain of the NAM that was implemented in the March 2008 change package. This expansion, primarily along the northern and eastern boundaries, was done at the request of NCEP's Aviation Weather Center and the National Weather Service's Alaska Region. A more efficient version of the WRF-NMM code was also implemented to mitigate the increase in resources needed to run the larger NAM domain.

2.2 *WRF-NMM Model: Gravity Wave Drag / Mountain Blocking*

For several years, most quantitative measurements have shown that the NAM has less skill in predicting large-scale synoptic patterns compared to the NCEP Global Forecast System (GFS). This is evident from Fig. 2, which depicts the NAM vs. GFS average 0-84 h 500 hPa RMS height errors and 250 hPa RMS vector wind errors over the CONUS and southern Canada for January-March 2006 (Eta Model/3DVAR in NDAS/NAM) and January-March 2007 (WRF-NMM/GSI analysis in NDAS/NAM). There was less difference in 250 hPa RMS vector wind error between the NAM and GFS when comparing January-March 2006 and January-March 2007. Little change was seen for 500 hPa heights between 2006 and 2007. The continuing NAM versus GFS skill differences led EMC to do a systematic evaluation of all differences between the two systems and to reduce these differences as much as possible. A full discourse on this topic and their impact on NAM vs. GFS skill are beyond the scope of this paper.

One critical component of the GFS that proved to be practical to put into the WRF-NMM is gravity wave drag / mountain blocking parameterization. The momentum transfer to the global momentum budget from the breaking of terrain-induced gravity waves has been shown in many studies (for example, Lilly *et al.*, 1982) to affect large-scale circulation patterns, especially at latitudes where orography is prominent (Miller *et al*., 1989).

The gravity wave drag parameterization in the GFS is described in Alpert *et al.* (1988, 1996) and Kim and Arakawa (1995). This was augmented by a sub-grid scale mountain blocking scheme to better simulate wind flow around sub-grid scale orography

(Alpert, 2004). This is based on the formulation of Lott and Miller (1997), which defines a dividing streamline below which air flows around the barrier. Above the dividing streamline, gravity waves can be generated and propagated vertically, depending on the stratification. For simplicity, we will use "GWD" to refer to the combined gravity wave drag / mountain blocking package. The GWD is formulated so that the influence of the sub-grid orography is scaled by a tuning parameter SIGFAC which, when multiplied by the standard deviation of the terrain, is added to the model terrain height to get an "effective" terrain height. After extensive tuning experiments in the 12-km WRF-NMM model with the modified NAM orography that is part of this change package (see below), best results were obtained with SIGFAC set to zero.

WRF-NMM forecast experiments with 10 examples of problematic NAM performance during 2006-2007 revealed that the inclusion of GWD can improve synoptic forecasts. An example of this is seen in Fig. 3, which shows the 72-h 500 hPa forecasts valid at the 1200 UTC 23 December 2006. In the GWD run, there are lower 500 hPa heights over eastern Canada and most of the eastern US than the control* WRF-NMM run, with a flatter, more progressive ridge over the mid-Atlantic states and New England. This led to an improved QPF forecast (Fig. 4a, b) in the GWD run over this region when compared to the verifying analysis (Fig. 4c).

2.3 *WRF-NMM Model: Unified Land-Surface Physics*

Another model component changed in the March 2008 NAM bundle was the land-surface physics. The original WRF Land-Surface Model (LSM) for the NMM was replaced by the Unified Noah Land-Surface Model (Tewari et al, 2008), developed jointly by EMC and NCAR. This new module was primarily a software enhancement and not a major physics upgrade. The only change to the physics that impacts the NAM is that the unified Noah LSM uses total soil moisture rather than liquid soil moisture (as in the previous version) to determine bare-soil evaporation. This leads to greater evaporation over frozen soil with patchy or no snow cover. Even with this change, tests of the new module (not shown) revealed no significant differences in near-surface fields in the warm season and small differences in the cold season.

2.4 *WRF-NMM Model: Advection of Passive Substances*

The horizontal and vertical advection for passive substances (specific humidity, cloud water, turbulent kinetic energy) in the WRF-NMM is performed by an updated version of the scheme developed for the NCEP Eta model by Janjic (1997). The procedure consists of a three step process. First, the first order upstream advection scheme is applied, which is positive definite for Courant numbers less or equal to one. Second, an optimized anti-filtering step is applied to restore gradients. After the anti-filtering step, conservation is again imposed on the combined changes from the advection and anti-filtering steps.

In the original scheme, the advection equation for passive variables was conservative for cyclic boundary conditions, closed domain, or rigid wall boundary conditions in combination with the continuity equation. Essentially, it assumed a closed system with no increase/decease of the total domain-integrated quantity. However, in the WRF-NMM forecast there is open inflow/outflow at the lateral boundaries. After some examination of the issue, it was apparent that it was physically incorrect to impose conservation on a system with open inflow/outflow at the lateral, upper, and lower boundaries. For this reason the scheme was changed to relax the requirement for exact conservation during the advective step.

WRF-NMM experiments with the modified advection on the 2006-2007 test cases showed improved QPF scores for precipitation amounts > 1 inch (not shown). An example can be seen in Fig. 5, which shows the 24-h QPF for the WRF-NMM forecast with both the modified advection and the gravity wave drag changes (compare to Fig. 4b). The heavier precipitation along the southeast US coast in Fig. 5 is attributable to the modified advection, which was closer to the observed 24-h amounts (Fig. 4c) along the South Carolina coast but predicted too much precipitation in southern Georgia and the Florida panhandle.

2.5 *WRF-NMM Model: Minor Changes*

Two minor changes to the WRF-NMM model's radiation scheme were made in the March 2008 NAM bundle. A bug was fixed in the computation of the climatological ozone values used in the model's radiation parameterization. The original version of the code applied the ozone values valid at the equator to all latitudes.

To address a cold bias in Arctic regions, two changes were made in the GDFL longwave radiation scheme in the original WRF-NMM in the NAM: 1) Longwave temperature tendencies from the lowest two model layers were averaged

---

* Disclaimer: Many of the experiments with the components of the NAM model changes discussed in this paper were done with the EMC WRF-NMM launcher, forecasts from which are usually initialized off the operational NAM analysis, and usually on a integration domain covering North America but smaller than the operational domain. The control runs described in this paper using the WRF-NMM launcher are a reasonable proxy for the operational NAM forecast.

together in order to address concerns that the layers might be too thin for the scheme to provide accurate heating/cooling rates; 2) The upward longwave radiation at the surface, originally based on the skin temperature, was changed to be computed from the average of the skin temperature and the lowest model layer temperature. The purpose of the latter change was to slow the rate that downward longwave radiation decreases when stable PBL conditions develop in clear skies.

These longwave changes were put into the NAM version of the WRF-NMM during its preliminary development in late 2005. After the June 2006 implementation, it became clear as the winter of 2006 approached that changes put into the surface layer and land-surface physics before the June 2006 WRF-in-NAM implementation had in some part already addressed this Arctic region cold bias. In December 2006, two changes were made in the NAM's microphysics which increased the amount of supercooled liquid water in the Arctic region, leading to higher incoming surface longwave radiation and a warm 2-m temperature bias in Alaska and Arctic Canada. Since the two longwave radiation changes, originally intended to mitigate a cold bias, were now making a warm bias worse, they were removed in the March 2008 NAM change package.

2.6 *GSI Analysis Changes*

Several changes were made to the GSI analysis for the March 2008 NAM change package. An updated release of the code (August 2007) was used which had several modifications, including analyzing surface pressure directly instead of the natural log of surface pressure, using height observations directly in the forward model instead of converting them to pressure, and using sensible temperature directly if an observation has no accompanying specific humidity observation.

Additionally, the background error covariances were retuned to account for model/analysis changes that were done since they were first estimated during the testing phase of the regional GSI analysis prior to the June 2006 implementation. The method used is described in Wu (2005). The impact of the retuned background errors in analysis performance is shown in Fig. 6. This figure shows time series of the surface pressure (top) and wind (bottom) observation RMS fit to the first guess for 140 consecutive 3-hourlly NDAS analyses during the fall of 2006. Use of the retuned background errors led to a better fit to the wind observations. The improvement in the fit to the surface pressure observations can be attributed to the tightening of the background error for the winds so that the analysis drew closer to the wind observations, resulting in a better fit to the surface pressure data.

Another aspect of the NAM versus GFS differences that can be reasonably addressed is to turn on new data types in the regional GSI that are being used in the global GSI analysis. Several new observation types have been turned on in the regional GSI analysis as part of the March 2008 NAM change package. These are 1) infrared cloud drift and water vapor winds above 600 hPa from the Moderate Resolution Imaging Spectroradiometer (MODIS), 2) infrared and visible cloud drift winds from METEOSAT-7, 3) surface mesonet winds on the NCEP use list (about 10% of all available sites), 4) single field-of-view GOES satellite radiances, and 5) radiances from the Atmospheric Infrared Sounder (AIRS).

NDAS tests during February-July 2007 of each new observation type (not shown) revealed neutral or small positive impact on GSI analysis performance. Fig. 7 shows the impact of assimilating AIRS radiances on the penalty function for conventional data at the end of each NDAS cycle for 35 cases in the spring of 2007. These plots show that the assimilation of AIRS data in the NDAS leads to a smaller penalty function (and better fit to the first guess) for conventional mass and wind observations. A full NDAS/NAM parallel test of the AIRS data during November-December 2006 (not shown) revealed small positive impact on the cumulative forecast RMS errors versus rawinsondes over the CONUS, with the greatest impact in the 500-300 hPa layer.

2.7 *NDAS Precipitation Assimilation*

Assimilation of observed precipitation in the NDAS was first implemented in 2001, using hourly observed precipitation over the CONUS. The original configuration and subsequent refinements during the Eta Model era of the NAM are described in Lin *et al*. (2001), Lin and Mitchell (2004) and Lin *et al*. (2004). In the final set of changes to the NAM/Eta Model done in May 2005 (Rogers *et al.*, 2005) the scheme was scaled back to only modify NDAS forecast latent heat and moisture fields when model precipitation is greater than the observed precipitation ($P_{mod} > P_{obs}$). To avoid negative impact on the NDAS soil moisture, the hourly observed precipitation (partitioned to physics time steps) replaced the model forecast precipitation as the driver to the model soil moisture.

In anticipation of increasingly sophisticated model physics in the WRF and future NWP architectures, the scheme was simplified further for WRF-in-NAM implementation in June 2006 by dropping the component that modified model moisture and latent heating when $P_{mod} > P_{obs}$. The hourly precipitation analysis used as a driver for NDAS soil moisture is a merged Stage II/IV product (Lin and Mitchell 2004), adjusted for biases using a long-term precipitation budget. When/where the precipitation analysis is not available (e.g., outside the CONUS (OCONUS)), or when it is snowing (a large low bias in hourly observed precipitation), the NDAS model 3-hour forecast precipitation is used

to drive the model's soil moisture. This can lead to excessive OCONUS soil moisture when there is a model precipitation spin-down problem, as was observed in the Eta and WRF-NMM models. The solution, implemented in the March 2008 NAM bundle, was to use the 12-36 hour 0000 UTC NAM forecast precipitation to drive the NDAS soil moisture outside of the CONUS. A comparison of July 2006 NDAS precipitation (sum of all 3-h forecasts) versus the sum of all operational NAM 12-36 h precipitation forecasts for the same month (Fig. 8) shows very high amounts in the NDAS outside of the CONUS due to the NDAS model precipitation spin-down.

Fig. 9 depicts the operational and parallel NAM 100-200 cm volumetric soil moisture valid 1200 UTC 4 February 2008. The parallel NAM shown ran with the OCONUS precipitation adjustment for about 1 year. It shows drier and more realistic soil moisture over Mexico and the Canadian Prairie Provinces.

2.8 *Model Terrain Changes*

The original model terrain in the WRF-NMM version of the NAM was based on the grid-cell mean computed from the 30" input data, with one pass of a peak smoother. Observations/complaints that the forecast model was too "noisy" during the assimilation prompted an investigation which led to changes in the model surface terrain implemented as part of the Match 2008 NAM change package. The new model terrain is created using two smoothing steps: 1) a 1-2-1 filter at every grid point, which will eliminate 2-delta-x noise by reducing the amplitude of large scale terrain features, and 2) a "de-smooth" step to restore some of the detail lost in step 1 at scales > 2-delta-x. For the NAM 3 passes of the filter are applied. Tests (not shown) revealed that use of the new smoothing led to a 3x decrease in the noise as measured by the domain-integrated square of the divergence tendency (Pyle, 2008 personal communication).

Other minor changes to the model terrain / land-sea mask includes a smaller (and more realistic) Great Salt Lake, a better depiction of the Channel Islands off the California coast, removal of spurious elevated water points, and the use of climatological water temperatures for Lake Champlain, provided by the Burlington, VT NWS Office (Sisson, 2007 personal communication).

2.9 *Quantitative Skill Scores and a Forecast Example*

Extensive real-time and retrospective testing of the full March 2008 NAM change package was performed. The periods tested were:

- NAM real-time parallel: 29 November 2007 to 30 March 2008
- NAM retrospective tests: March, August 2007

Fig. 10 shows the day 1, 2, and 3 cumulative CONUS RMS height, temperature, vector wind, and relative humidity errors versus rawinsondes for all pressure levels from November 2007-March 2008 for the operational and parallel NAM. The parallel NAM statistics are uniformly better at all levels and forecast hours, with the biggest improvement seen in upper troposphere height/wind and lower troposphere temperature. Similar improvement was seen over Alaska (not shown). The impact of the changes on 24-h QPF equitable threat and bias scores (not shown) was small. The full set of statistics is available at http://www.emc.ncep.noaa.gov/mmb/namchanges_winter2008/nam_upgrades.2008.html and http://www.emc.ncep.noaa.gov/mmb/mmbpll/paralog/paralog.namx_opspll.html .

Fig. 11 shows an example of an operational NAM "dropout" case where the parallel NAM running the March 2008 change package had an improved 500 hPa forecast. Time series of the cumulative 36-h forecast 500 hPa RMS height errors over the CONUS and southern Canada (not shown) revealed that the operational NAM forecast valid 0000 UTC 26 December 2007 had an error nearly 40% higher than the parallel NAM. Fig. 11 shows that the operational NAM forecast (top left) predicts a nearly in-phase trough extending from Hudson's Bay southward into the Texas panhandle. The parallel NAM (top right) and operational GFS (bottom left) predicted the southern part of the hanging back and beginning to cut off over New Mexico, a more realistic solution as seen when the forecasts are compared to the verifying GDAS analysis (bottom right).

3. 16 DECEMBER 2008 CHANGES

An online description of each component of the December 2008 NAM changes can be found at http://www.emc.ncep.noaa.gov/mmb/mmbpll/briefings/NAM_December2008-1.pdf .

3.1 *WRF-NMM Model: Land-surface physics*

Several problematic cold-season NAM forecasts of 2-m dew point temperature over snow cover have led to two changes in the Unified Noah LSM physics running in the WRF-NMM. Fig. 12 shows a 21-h control WRF-NMM forecast of 2-m dew point temperature valid 0900 UTC 9 January 2007. There are two regions of very low 2-m dew point temperature over the Sierra Nevada Mountains in California and in southern Colorado. Both locations are in areas where the stability (as measured by the Bulk Richardson number) is large over snow covered areas. The original algorithm in the unified LSM produced excessively large frostfall on the surface which led to a collapse of the 2-m dew point temperature to as low as -80^{o}C. To alleviate this problem, in situations when the potential evaporation (PE) is negative over snow cover, PE is limited by forcing it to decrease with increasing

surface layer stability (via a linear decrease as a function of Bulk Richardson number), weighted by snow coverage. The WRF-NMM forecast with the modification (Fig. 13) shows that the 2-m dew point temperatures in the two problem areas are significantly higher.

The second change to the LSM addressed a problem with excessive fog in daytime over snow covered regions. This was caused by the potential evaporation rising unrealistically as the air temperature rose, but the snowpack would keep the surface at the freezing point until all the snow melted. The solution was to let the slope of the saturation humidity function with respect to temperature decrease linearly with snow cover. This led to improved daytime 2-m dew point temperature forecasts (not shown) along the edge of the melting snowpack.

3.2 *WRF-NMM Model: Radiation/Clouds*

Observations from the EMC Land-Surface modeling group (Ek, 2008 personal communication) indicated that the WRF-NMM model had a high downward shortwave surface flux bias during the winter of 2007-08. This led to speculation that the model clouds might be allowing too much solar radiation to pass through them. A poor NAM forecast for a freezing rain event in the Washington, DC area in February 2008 led to an investigation to see it this problem might be playing a role in some problematic NAM winter weather forecasts.

Fig. 14 shows the RUC analysis and control WRF-NMM 12-h forecast of 2-m temperature valid 0000 UTC 13 February 2008. Significant cold-air damming is seen in the RUC analysis over Maryland and Virginia east of the Appalachians. At 0000 UTC 13 February freezing rain/drizzle was falling along an axis from Baltimore, MD southwestward through Washington, DC and into central Virginia (not shown). As Fig. 14 shows, the control WRF-NMM forecast did not predict the strength of the cold-air damning, with freezing line north of the Washington, DC metro area.

To address this problem in the context of the model's radiation physics and the interaction with model clouds, the cloud optical thicknesses were increased by effectively doubling the absorption coefficients for water and ice in the radiation parameterization. The WRF-NMM test run with this change (Fig. 15) had more pronounced cold air damming over the mid-Atlantic region, but was still underdone. WRF-NMM forecast runs with the 2006-2007 test cases (not shown) showed neutral or small positive impact over the CONUS. WRF-NMM test runs over Alaska with this modification had a mixed impact in that the change produced cooler surface temperatures during the warm season, enhancing an existing cool bias, while it produced warmer surface temperatures in the cold season, when the NAM was also too cool.

3.3 *WRF-NMM Model: Other Changes*

Two additional changes were made to the WRF-NMM model:

1) The PBL/turbulence schemes were modified to mix each hydrometeor species in the vertical, the previous version only mixed cloud water

2) To apply vertical diffusion for separate water species, the model was changed so that (a) it can apply vertical diffusion to an arbitrary number of species, and (b) the counter gradient option can be applied to some or all of the species if desired.

WRF-NMM tests (not shown) showed small impact from these changes.

3.4 *GSI Analysis Changes*

Several changes were also made to the GSI analysis for the December 2008 NAM change package. A new (Fall 2008) version of the GSI code was implemented, which included an updated version of the Joint Center for Satellite Data Assimilation's (LeMarshall *et al.* 2007) Community Radiative Transfer Model (CRTM, Han *et al.*, 2006). Test of this new code (not shown) had a small positive impact on analysis performance. The new version of CRTM uses default climatology in the upper atmosphere. The previous version just used the first guess values themselves. The new CRTM with the default climatology improved the assimilation of satellite radiances because the NAM's model top pressure of 2 hPa is too low for the radiative integration. With a deep layer between the NAM model top pressure of 2 hPa and 0.005 hPa (the top pressure in the CRTM), the integration was an ill-posed mathematical problem.

Also, new observation types were turned on in the regional GSI in December 2008: 1) Tropospheric Airborne Meteorological Data Reporting (TAMDAR, Daniels *et al*., 2006) aircraft temperature/moisture data over the CONUS and Alaska, 2) Canadian AMDAR aircraft temperature data, and 3) satellite radiances from the European Organization for the Exploitation of Meteorological Satellites (EUMETSAT) MetOp-a satellite. NDAS tests with the TAMDAR/AMDAR data resulted in a small improvement in the first guess fit of rawinsonde data (Fig.16). Test with the MetOp data (not shown) had a neutral impact.

3.5 NDAS Changes : Partial cycling

The NDAS and its predecessor, the Eta Data Assimilation System (EDAS) have been a fully self-contained cycling system since July 1998, with all atmospheric and land-state variables cycled from the previous NDAS run. Other than updating the snow, sea ice, and sea surface temperature once per day, the only outside forcing is the use of the best available NCEP global model forecast to

provide lateral boundary conditions to the NDAS and NAM forecasts. From February 1998 (Rogers *et al.* 1998) to July 1998, the EDAS used "partial cycling" in which only soil fields, cloud parameters, and turbulent kinetic energy (TKE) are fully cycled. With partial cycling, the atmospheric variables used as background for the first EDAS analysis were taken from a 6-hour forecast of the NCEP Global Data Assimilation System (GDAS). Even after full EDAS/NDAS cycling was implemented in July 1998, the partial cycling option would be invoked in NCEP operations if the NDAS first guess was not available due to NDAS failures caused by hardware or software problems. This was a very rare occurrence, happening no more than once or twice.

Although the March 2008 changes improved NAM performance, the magnitude of the NAM versus GFS differences were only marginally reduced (not shown). For many years it has been observed by EMC researchers that WRF-NMM forecast experiments initialized from the GDAS/GFS initial conditions generally produced better synoptic-scale forecasts than those from the NDAS/NAM initial conditions. This option would not be practical in NCEP operations since the GFS runs about 90 minutes later than the NAM. Also, running the NAM solely off a global analysis without the cycled land states from the NDAS (with the direct driving of the land-surface physics by the observed precipitation) would undoubtedly degrade near-surface forecasts. However, what would be practical in an operational environment is to revisit the partial cycling option, which uses the GDAS forecast as the atmospheric first guess for the first NDAS analysis of each cycle.

For the purposes of this discussion, we shall call using the GDAS forecast to initiate the 12-hour NDAS as "NDAS Partial Cycling (NPCY)". During the pre-implementation testing for the March 2008 NAM change package, EMC ran an additional parallel NAM test with the NPCY method. Fig. 17 shows cumulative 24-h (black lines), 48-h (red lines), and 72-h (blue lines) RMS errors of height, temperature, relative humidity, and vector wind from 17 December 2007 – 25 February 2008 over the CONUS and southern Canada for three NAM runs: the operational NAM (solid), the parallel NAM running the March 2008 changes (dashed), and the parallel NAM running the March 2008 changes with the NPCY method (long dash-dot). For height and vector wind, using the NPCY method led to an incremental reduction in RMS error at all pressure levels at 48-h and 72-h, with the greatest impact in the 250-300 hPa layer. For temperature, the greatest improvement is seen in the middle troposphere between 700 and 400 hPa.

Based on the above results, it was decided to implement the NPCY option to initialize the NDAS in the December 2008 NAM change package. It should be pointed out that the use of partial cycling in the NDAS is considered a temporary solution to improve NAM forecasts while more advanced techniques to control imbalances in the NDAS (such as strong mass-wind balance constraint in the GSI analysis or digital filter initialization in the model) are developed.

3.6 *AFWA Snow Depth Analysis*

The Air Force Weather Agency (AFWA) snow depth analysis (Kopp *et al*., 1996) used in the NDAS/NAM was upgraded from the 1/8th mesh product (~45 km resolution) to the 1/16th mesh product (~23 km resolution). The analysis uses microwave-based detection algorithms, in-situ observations, and climatology to determine snow depth. The change showed no negative effects, and was necessary since the coarser resolution product will be shut down in the future.

3.7 *Quantitative Skill Scores and Forecast Examples*

Real-time and retrospective testing of the December 2008 NAM change package was performed for these time periods:

- NAM real-time parallel: 1 October 2008 – 16 December 2008
- NAM retrospective test: March 2007; the control run for this retrospective test was the parallel NAM retrospective test for March 2007 run for the March 2008 change package, described in Section 2.9.

The cumulative CONUS and Alaska RMS errors for the real-time and retrospective parallels show a similar reduction to the RMS errors that was seen in the December 2007 – March 2008 example (Fig. 17), and thus are not shown. Fig. 18 shows the 24-h QPF equitable threat score (ETS) and bias score for the March 2007 retrospective (left) and the October-December 2008 real-time parallel. Lower bias is evident for both periods, as it was seen in tests for the warm season during the summer of 2008 (not shown). Surface statistics for the parallel NAM (not shown) are generally better than those from the operational NAM, with a daytime warm bias reduced in the eastern half of the CONUS and a nighttime cool bias reduced slightly in the western CONUS. More details are available at http://www.emc.ncep.noaa.gov/mmb/mmbpll/briefings/NAM_December2008-1.pdf and at http://www.emc.ncep.noaa.gov/mmb/mmbpll/paralog/paralog.namx_fall2008.html .

It was observed during parallel testing that the NAM parallel w/partial cycling would at times more resemble the GFS forecast than the operational NAM, especially during the latter part of the forecast. Fig. 19 shows the time series from 4-18 October 2008 of 72-h forecast 500 hPa RMS height error and height bias error valid at 0000 UTC for the operational NAM, operational GFS, and the parallel NAM (labeled NAMX). Overall, for this particular

two week period the operational NAM RMS error was about 15% worse than the GFS, while the parallel NAM errors were about 9% higher than the GFS. Three 500 hPa height forecast examples from the NAM, parallel NAM (plotted as NAMX), and GFS during this period are presented in Figs. 20-22. Fig. 20, a 72-h forecast valid 0000 UTC 8 October 2008, shows that NAMX had a better forecast of the 500 hPa short-wave trough over the central US than the NAM and especially the GFS, which predicted a erroneous closed 500 hPa low over Kansas and Arkansas. Fig. 21, an 84-h forecast valid 0000 UTC 12 October 2008, shows that all three models predicted the cutoff low over the southwestern US, but the operational NAM had the low positioned too far to the southwest. In both these cases the NAMX more closely resembled the GFS. When the GFS has a "dropout" forecast, however, NAMX can as well, as seen in Fig. 19 which shows that the GFS 72-h RMS height error valid 0000 UTC 14 October is about 20% higher than the operational NAM, while the parallel NAM was even worse than the GFS. Fig. 22 shows the 500 hPa height forecasts for this time, when the position of the 500 hPa low along the US-Canadian border was too far to the west in the GFS and NAMX forecasts.

4. CONCLUSION AND FUTURE PLANS

The overall impact of the March 2008 and December 2008 changes on the NAM versus GFS differences can be seen in Fig. 23, which shows the NAM and. GFS average 0-84 h 500 hPa RMS height and 250 hPa RMS vector wind errors over the CONUS and southern Canada for January–March 2009. When compared to the same 3 month period in 2006 and 2007, by 84-h the NAM 500 hPa RMS height error is ~20% less. The NAM's 250 hPa wind errors have improved to the point where they are nearly identical to the GFS by 84-h.

The December 2008 NAM implementation is the last major set of changes to the WRF-NMM-based NAM. In 2010, the NAM modeling infrastructure will be changed to run within the Earth Science Modeling Framework (ESMF)-based NOAA Environmental Modeling System (NEMS) framework (Black *et al*., 2009, paper 2A.6). The NMM model will be replaced with the NCEP Nonhydrostatic Multiscale Model (NMMB, Janjic, 2009, paper 5A.1). In addition to the current 12-km NAM 84-h forecast over North America, two ~3-6 km resolution runs over the CONUS and Alaska will run nested inside the 12-km NAM. Additional details can be found in the above two papers at this conference and in Lapenta *et al.* (2009, paper 2A.5).

5. REFERENCES

Alpert, J., M. Kanamitsu, P. Caplan, J. Sela, G. White, and E. Kalnay, 1988: Mountain induced gravity wave drag parameterization in the NMC Medium-Range Forecast Model. *Proc. 8th Conference on Numerical Weather Prediction,* AMS, Baltimore, MD, 726-733.

Alpert, J., S.-Y. Hong, and Y.-J. Kim, 1996: Sensitivity of cyclogenesis to lower troposphere enhancement of gravity wave drag using the Environmental Modeling Center Medium Range Model. *Proc. 11th Conference on Numerical Weather Prediction*, American Meteorological Society, Norfolk, VA, 322-323.

Alpert, J., 2004: Sub-grid scale mountain blocking at NCEP. *Proc. 20th Conference on Weather Analysis and Forecasting/17th Conference on Numerical Weather Prediction*, American Meteorological Society. Seattle, WA.

Black, T., H.M.H. Juang, and M. Iredell, 2009: The NOAA Environmental Modeling System at NCEP. *Proc 23rd Conference on Weather Analysis and Forecasting/19th Conference on Numerical Weather Prediction*, American Meteorological Society, Omaha, NE.

Daniels, T., W. Moninger, and R. Mamrosh, 2006: Tropospheric Airborne Meteorological Data Reporting (TAMDAR) overview. *Proc 10th Symposium on Integrated Observing and Assimilation Systems for Atmosphere, Ocean, and Land-Surface*. American Meteorological Society, Atlanta, GA.

Han, Y., P. van Delst, Q. Liu, F. Wang, B. Yan, R. Treadon, and J. Derber, 2006: Community radiative Transfer Model (CRTM) – Version 1. NOAA Technical Report # 122.

Janjic, Z., 1997: Advection scheme for passive substances in the NCEP Eta Model. *Research Activities in Atmospheric and Oceanic Modeling*, WMO, Geneva, CAS/JSC WGNE, 3.14.

Janjic, Z., 2003: A nonhydrostatic model based on a new approach. *Meteor. Atmos. Phys.,* **82**, 271-285.

Janjic, Z., T. Black, M. Pyle, H.-Y. Chuang, E. Rogers, and G. DiMego, 2005: The NCEP WRF model core. *Proc. 21st Conference on Weather Analysis and Forecasting/17th Conference on Numerical Weather Prediction*, American Meteorological Society, Washington, DC.

Janjic, Z., 2009: Further development of a model for a broad range of spatial and temporal scales. *Proc 23rd Conference on Weather Analysis and Forecasting/19th Conference on Numerical Weather Prediction*, American Meteorological Society, Omaha, NE.

Kim, Y.J., and A. Arakawa, 1995: Improvement of orographic gravity wave drag parameterization using a mesoscale gravity wave model. *J. Atrmos. Sci*, **52**, 1875-1902.

Kopp, T., and R. Kiess, 1996: The Air Force Global Weather Central Snow Analysis Model. *Proc 15th Conference on Weather Analysis and Forecasting*, American Meteorological Society, Norfolk, VA.

Lapenta, W., S. Lord, J. Ward, G. DiMego, H. Tolman, J. Derber, H. Pan, N. Surgi, Z. Toth, and M. Ek, 2009: Recent advances in weather and climate prediction at the National Centers for Environmental Prediction. *Proc 23rd Conference on Weather Analysis and Forecasting/19th Conference on Numerical Weather Prediction*, American Meteorological Society, Omaha, NE.

LeMarshall, J., L. Uccellini, F. Einaudi, M. Colton, S. Chang, F. Wang, M. Uhart, S. Lord, L.-P. Riishoijgaard, P. Phoebus, and J. Yoe, 2007: The Joint Center for Satellite Data Assimilation. *Bull. Amer. Meteor. Soc,* **88,** 329-340.

Lilly, D.K., D.M. Chervin, P.J. Kennedy, and J.B. Klemp, 1982: Aircraft measurements of wave momentum flux over the Colorado Rocky Mountains. *Quart. J. R. Met. Soc.*, **108**, 625-642.

Lin, Y., M. Baldwin, K. Mitchell, E. Rogers, and G. DiMego, 2001: Spring 2001 changes to the NCEP Eta analysis and forecast system: Assimilation of observed precipitation. *Proc. 18th Conference on Weather Analysis and Forecasting/14th Conference on Numerical Weather Prediction*, American Meteorological Society, Ft. Lauderdale, FL, J92-J95.

Lin, Y., and K. Mitchell, 2004: The NCEP Stage II/IV hourly precipitation analysis: Development and Applications. *Proc. 19th Conference on Hydrology*, American Meteorological Society, San Diego, CA.

Lin, Y., K. Mitchell, E. Rogers, and G. DiMego, 2004: Using hourly and daily precipitation analyses to improve model water budget. *Proc. 9th Symposium on IOAS-AOLS*, American Meteorological Society, San Diego, CA.

Lott, F., and M.J. Miller, 1997: A new subgrid-scale orographic drag parameterization: Its formulation and testing. *Quart. J. Roy. Met. Soc.*, **123,** 101-127.

Miller, M.J., T.N. Palmer, and R. Swinbank, 1989: Parameterization and influence of subgridscale orography in general circulation and numerical weather prediction models. *Meteor. Atmos. Phys.,* **40**, 84-109.

Rogers, E., M. Baldwin, T, Black, K. Brill, F. Chen, G. DiMego, J. Gerrity, G. Manikin, F. Mesinger, K. Mitchell, D. Parrish, and Q. Zhao, 1998: Changes to the NCEP Operational "Early" Eta Analysis and Forecast System. NWS Technical Procedures Bulletin Number 447, available at http://www.nws.noaa.gov/om/tpb/447body.htm .

Rogers, E., Y. Lin, K. Mitchell, W.-S. Wu, B. Ferrier, G. Gayno, M. Pondeca, M. Pyle, V. Wong, and M. Ek, 2005: The NCEP North American Modeling System: Final Eta model / analysis changes and preliminary experiments using the WRF-NMM. *Proc. 21st Conference on Weather Analysis and Forecasting/17th Conference on Numerical Weather Prediction*, American Meteorological Society, Washington, DC.

Tewari, M., M. Ek, F. Chen, J. Dudhia, A. Kumar, K. Mitchell, G.-Y. Niu, Z.-L. Yang, D. Niyogi, X. Zeng, and J. Eylander, 2008: Release of the unified Noah land surface model in WRF3.0 and plan for future enhancements. *Proc. 9th Annual WRF User Workshop*, NCAR, Boulder, CO.

Wu, W.-S., R.J. Purser, and D.F. Parrish, 2002: Three-dimensional variational analysis with spatially inhomogeneous covariances. *Mon. Wea. Rev.*, **130**, 2905-2916.

Wu, W.-S., 2005: Background error for NCEP's GSI analysis in regional mode. *Proc 4th WMO International Symposium on Assimilations of Observations in Meteorology and Oceanography*, Prague, Czech Republic.

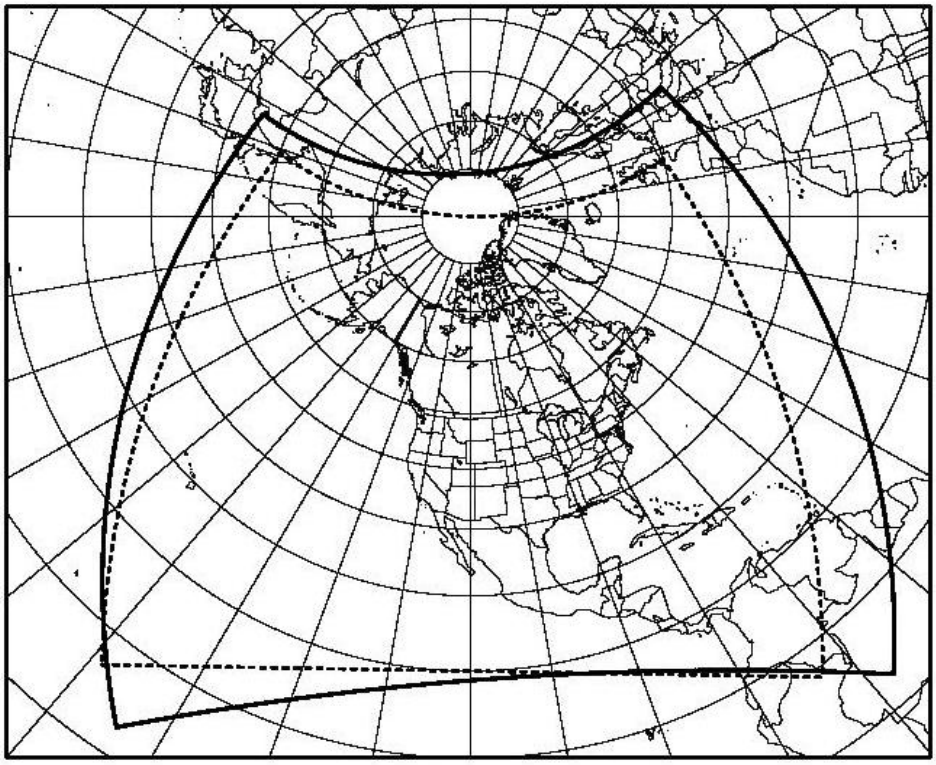

Figure 1: Expanded NAM domain implemented in March 2008 (solid); original NAM domain (dashed).

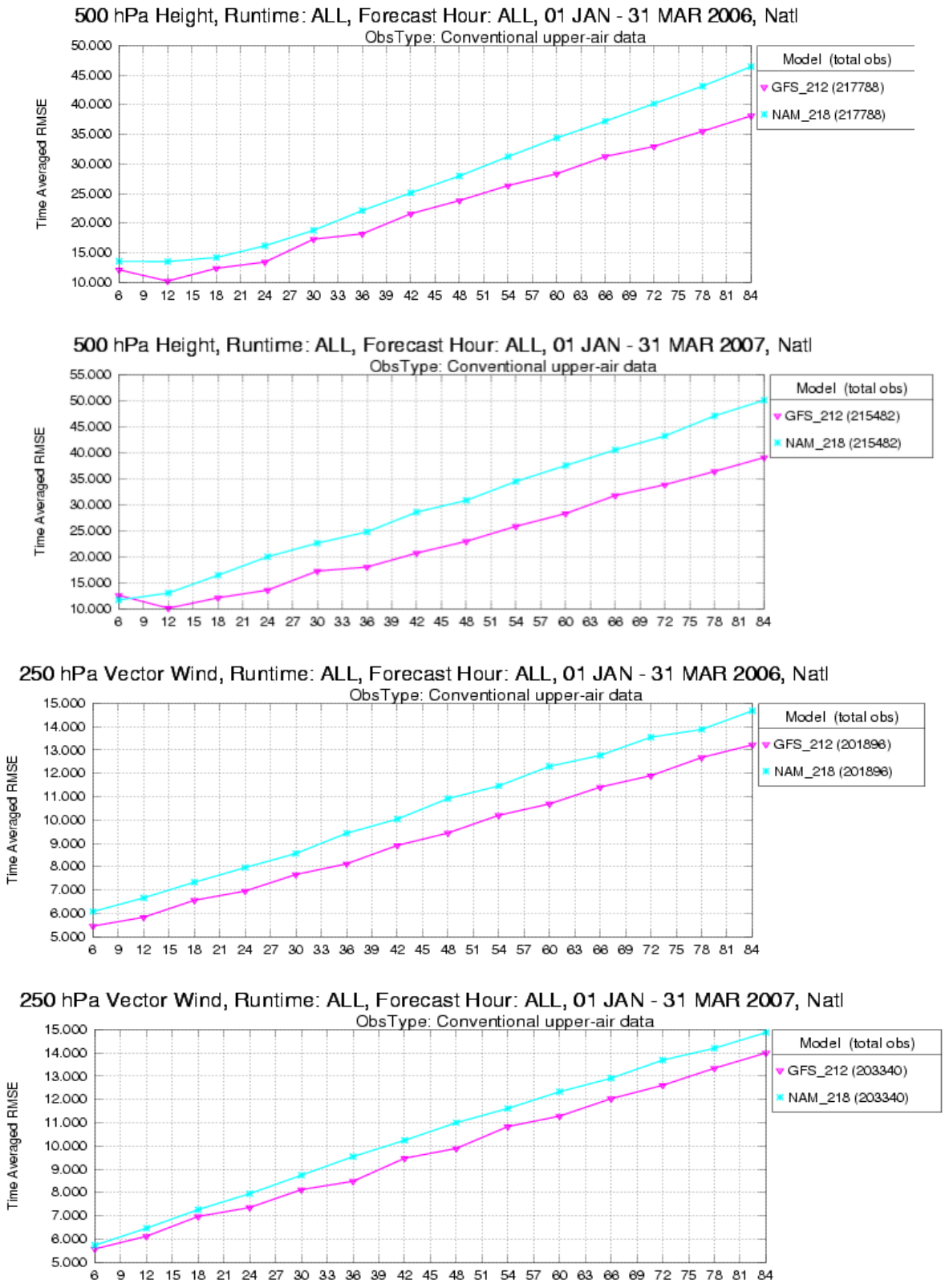

Figure 2: NAM (blue) vs. GFS (magenta) averaged 0-84 h 500 hPa RMS height errors (m, top 2 plots) and 250 hPa RMS vector wind errors (ms^{-1}, bottom 2 plots) over the CONUS for January – March 2006 and January-March 2007.

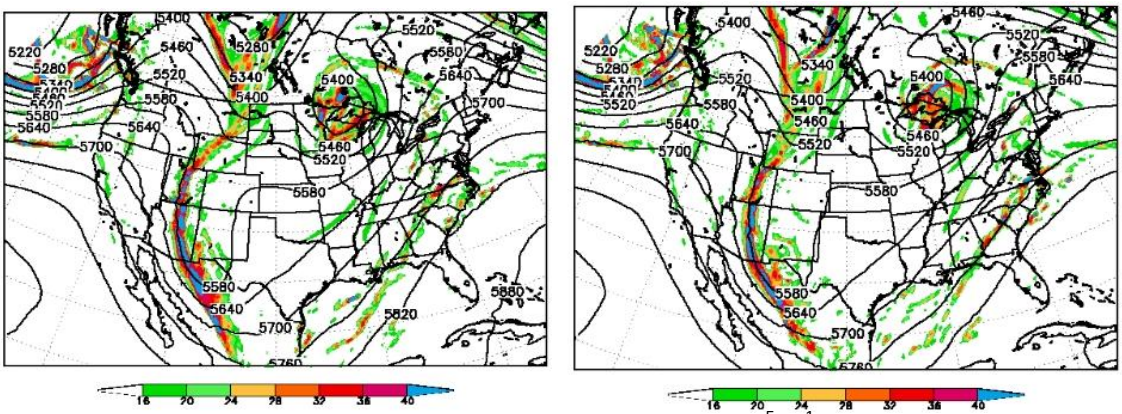

Figure 3: 72-h forecast 500 hPa height (m) and absolute vorticity (10^{-5} s^{-1}) forecast valid 1200 UTC 23 December 2006 for the control WRF-NMM (left) and the parallel WRF-NMM with gravity wave drag/mountain blocking (right).

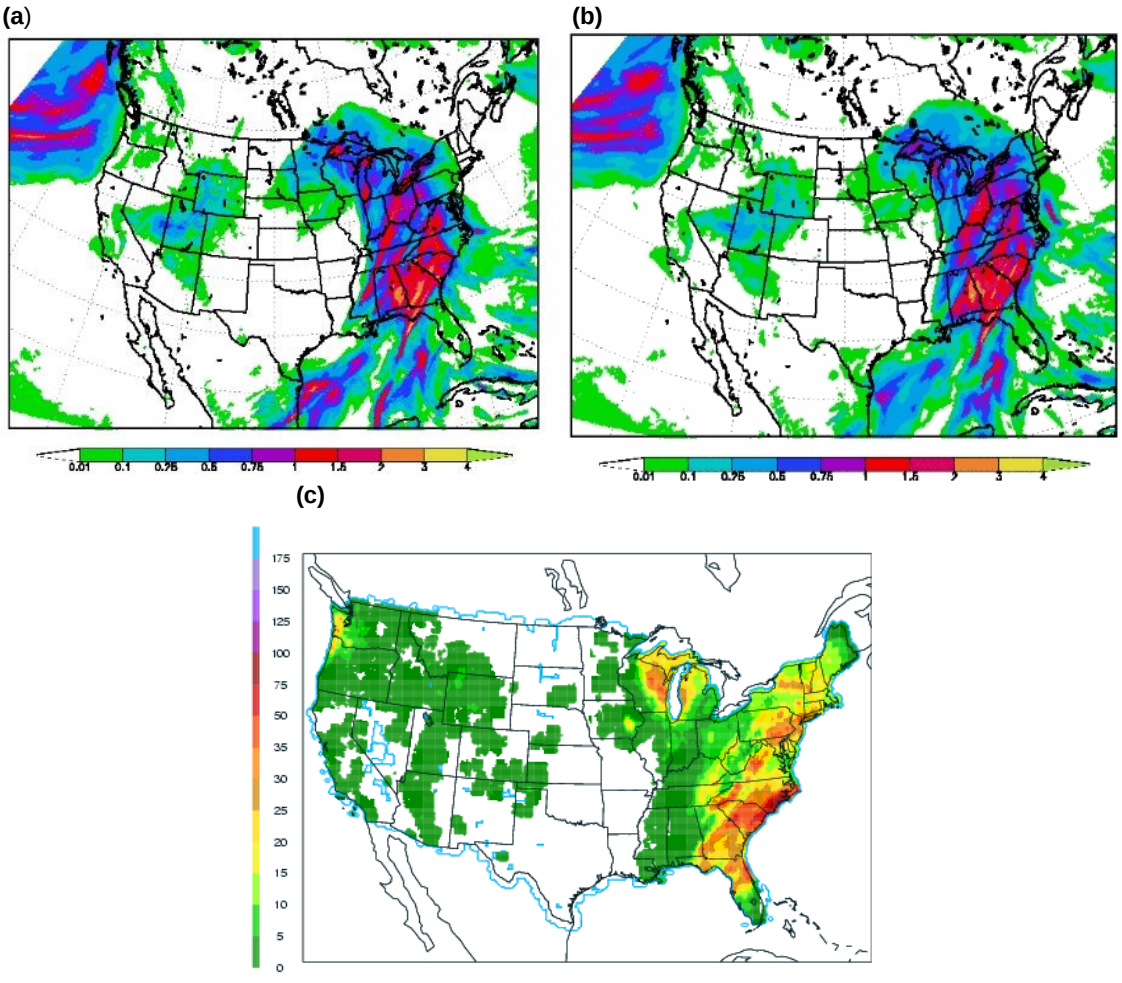

Figure 4: (a) 72-h forecast of 24-h accumulated precipitation (valid 1200 UTC 23 December 2006 for the control WRF-NMM run; (b) same as (a) but for the parallel WRF-NMM with gravity wave drag/mountain blocking, (c) NCEP CPC analysis of 24-h accumulated precipitation (mm) valid 1200 UTC 23 December 2006.

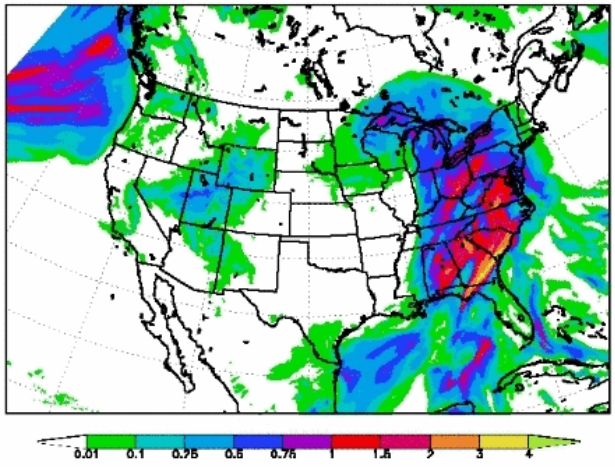

Figure 5: Same as Figure 4b, but for the parallel WRF-NMM forecast with modified advection and gravity wave drag/mountain blocking.

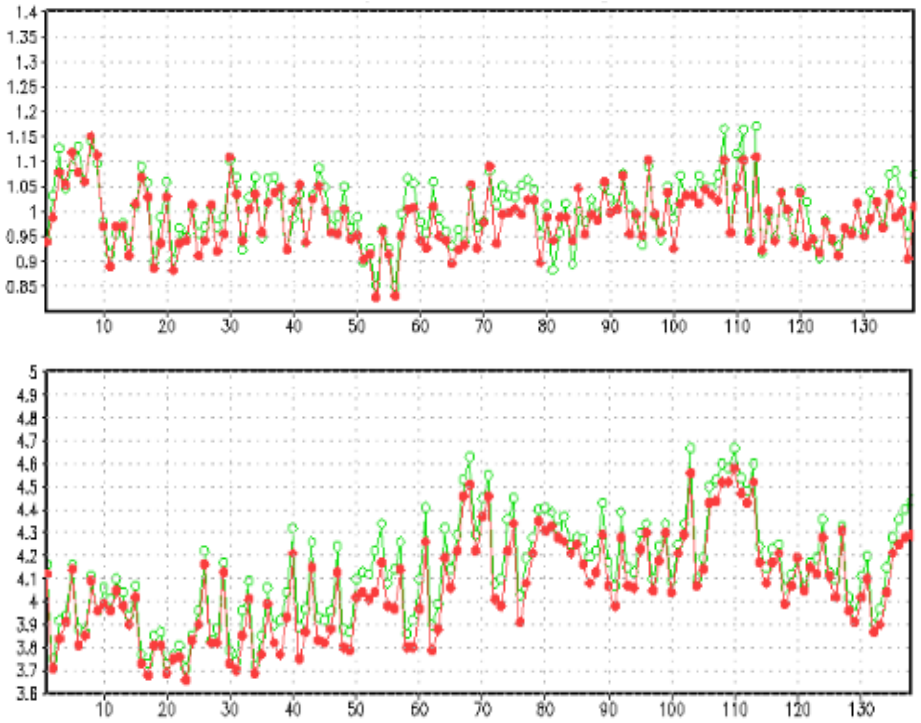

Figure 6: Time series of observation RMS fit to the NDAS first guess for surface pressure data (top, hPa) and vector wind (bottom, ms^{-1}) for the control NDAS (green) and parallel NDAS with the modified background error covariances (red) for 140 consecutive NDAS analyses during the fall of 2006.

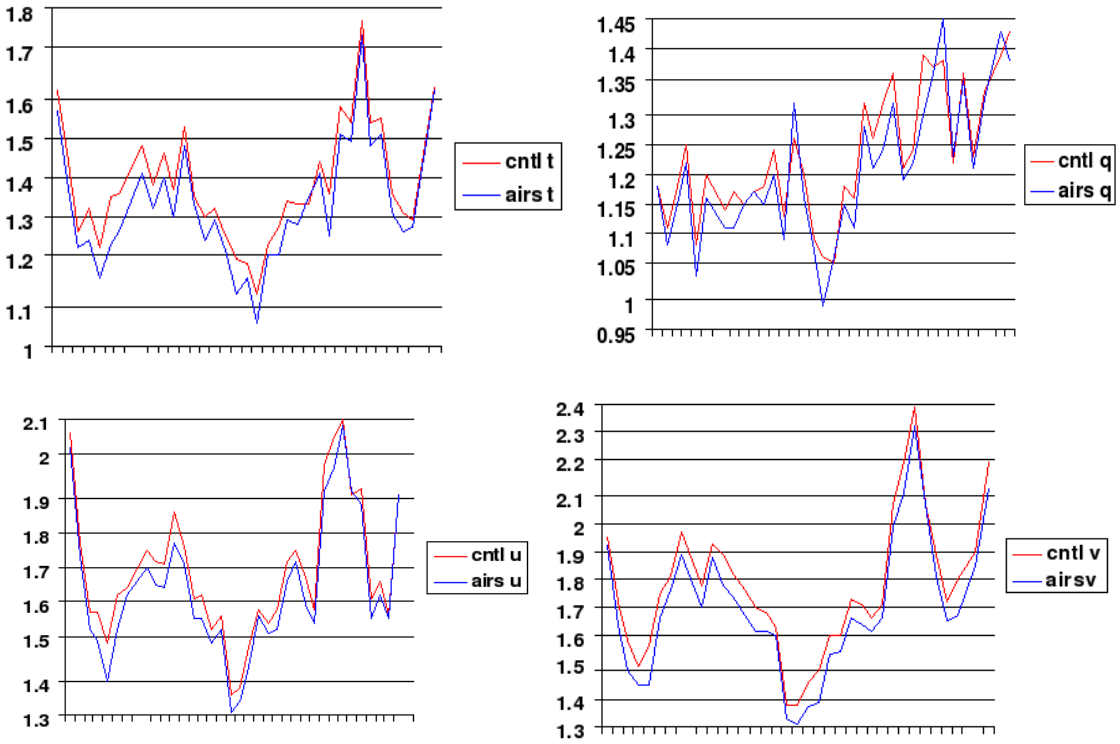

Fig. 7: GSI analysis penalty function for conventional data (vertical axis) for 35 NDAS cycles (horizontal axis) for temperature (top left), specific humidity (top right), u-component of wind (bottom left) and v-component of wind (bottom right) for the control NDAS (red) and parallel NDAS assimilating AIRS radiances (blue).

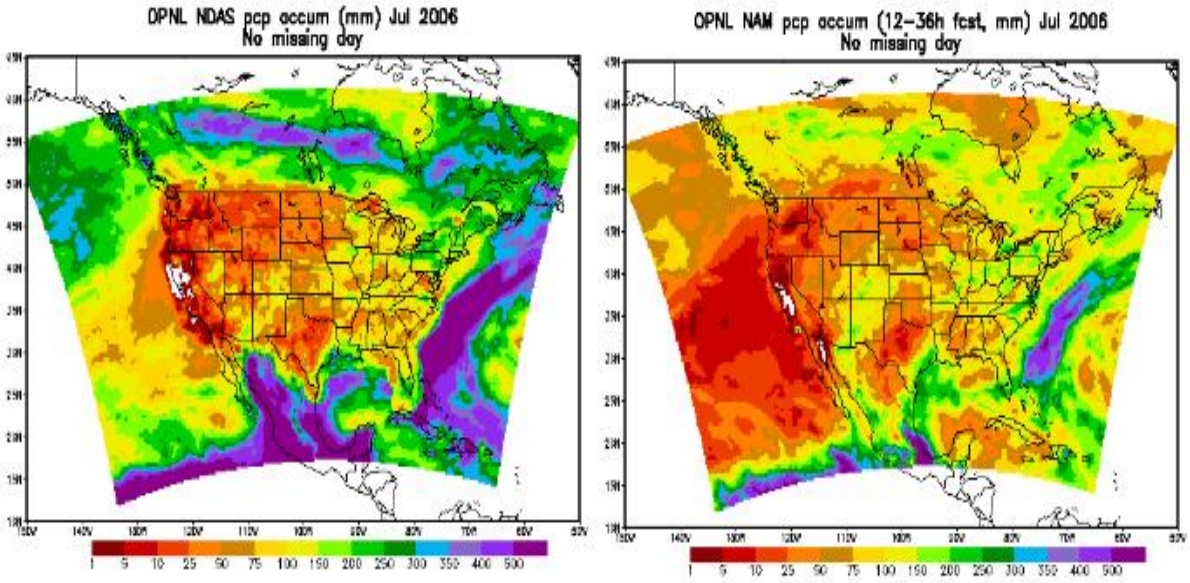

Figure 8: Left: Sum of accumulated precipitation (mm) of all 3-h NDAS forecasts during July 2006; Right: Sum of all operational NAM 12-36 h forecast accumulated precipitation (mm) during July 2006.

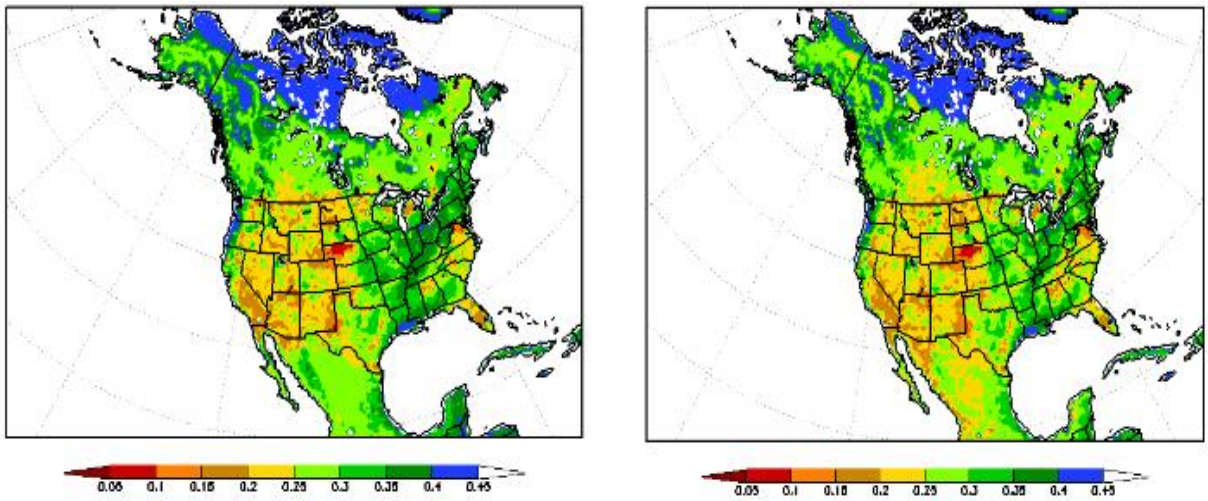

Figure 9: Operational (left) and parallel (right) NAM 100-200 cm volumetric soil moisture (precent/100) valid 1200 UTC 4 February 2008.

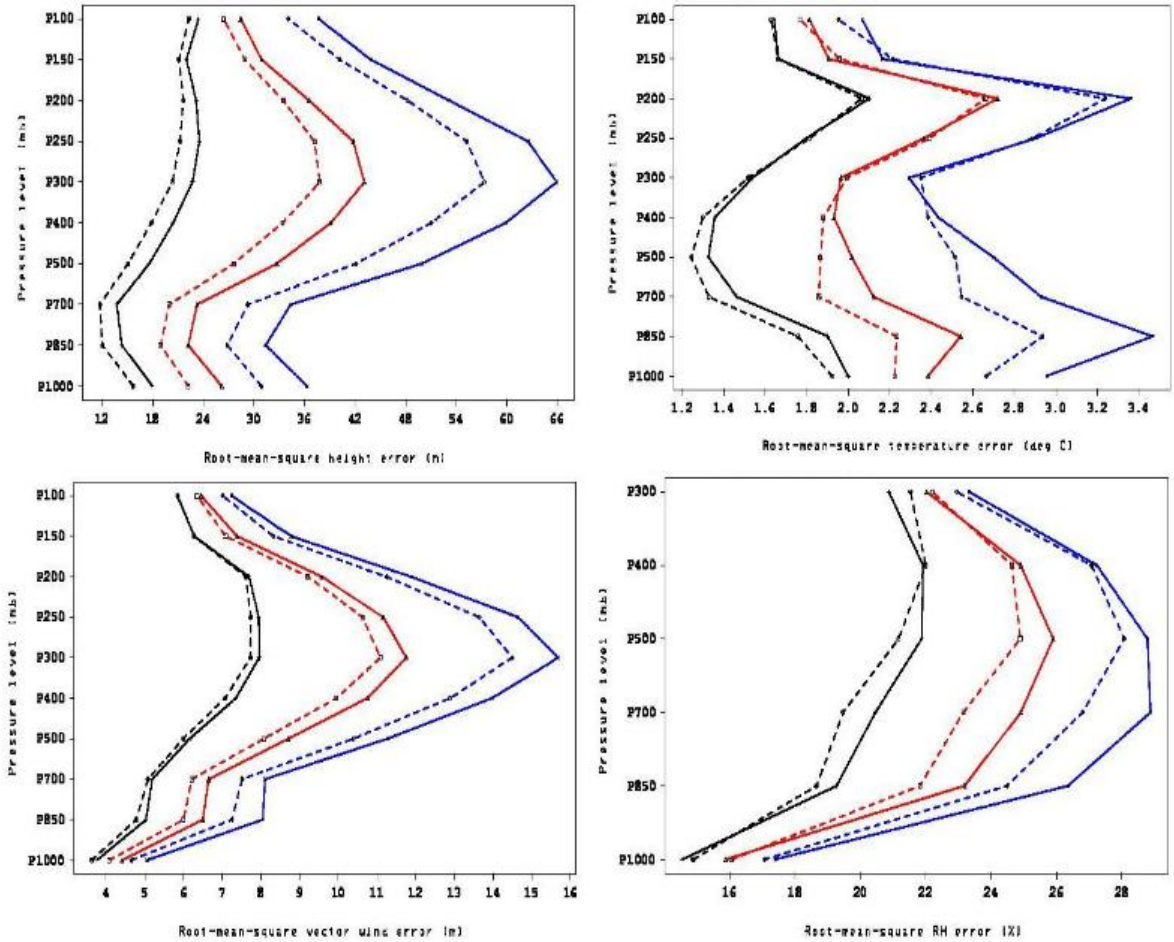

Figure 10: Operational NAM (solid) and parallel NAM with the March 2008 changes (dashed) cumulative RMS 24-h (black), 48-h (red) and 72-h (blue) forecast errors versus rawinsondes over the CONUS for height (m, top left), temperature (^{o}C, top right), vector wind (ms^{-1}, bottom left) and relative humidity (%, bottom right) for November 2007-March 2008.

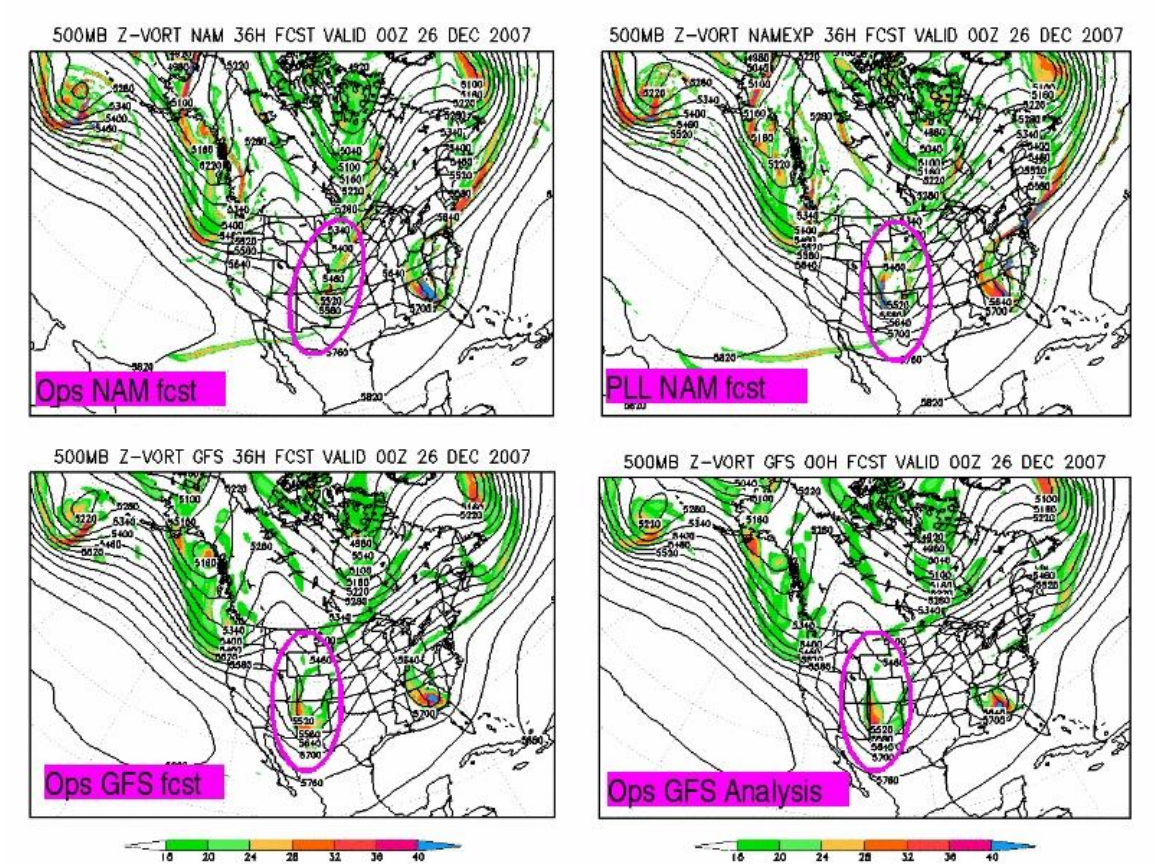

Figure 11: 500 hPa height (m) and absolute vorticity (10^{-5} s^{-1}) 36-h forecast valid 0000 UTC 26 December 2007 for the operational NAM (top left), parallel NAM w/March 2008 change package (top right), and operational GFS (bottom left). Verifying GFS analysis shown in the bottom right panel.

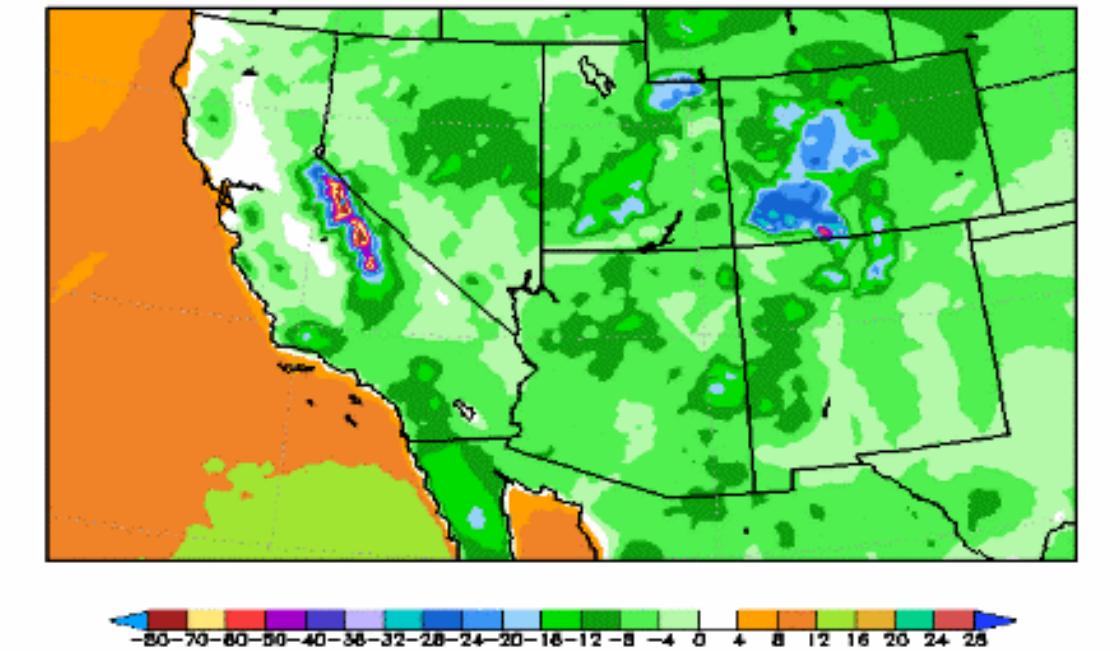

Figure 12: Control WRF-NMM 21-h forecast of shelter dew point temperature (^{o}C) valid 0900 UTC 9 January 2007.

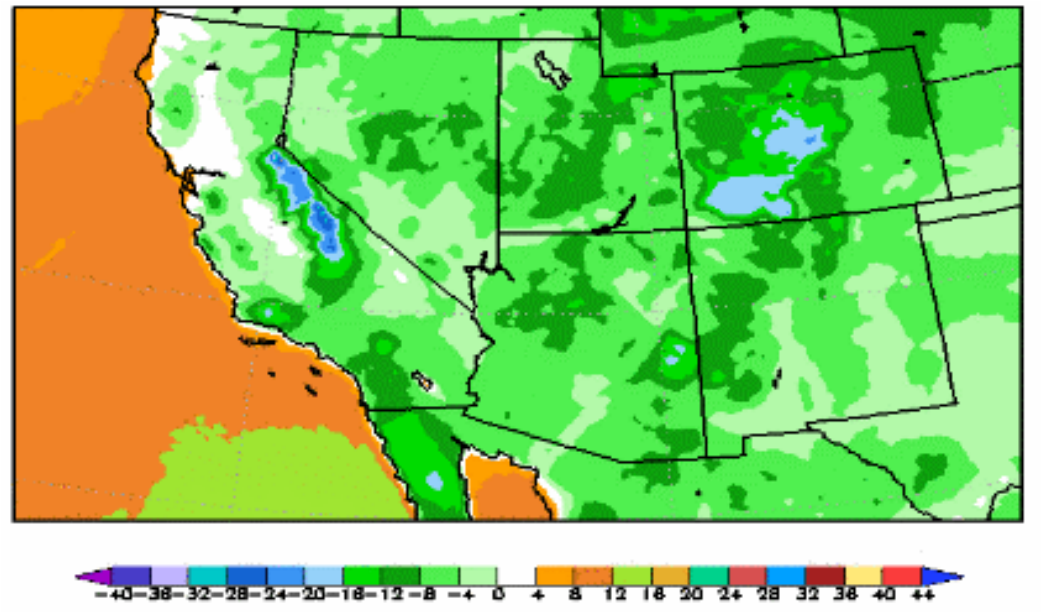

Figure 13: Same as Figure 12, but for a parallel WRF-NMM forecast with the modification to potential evaporation over snow cover in December 2008 NAM change package.

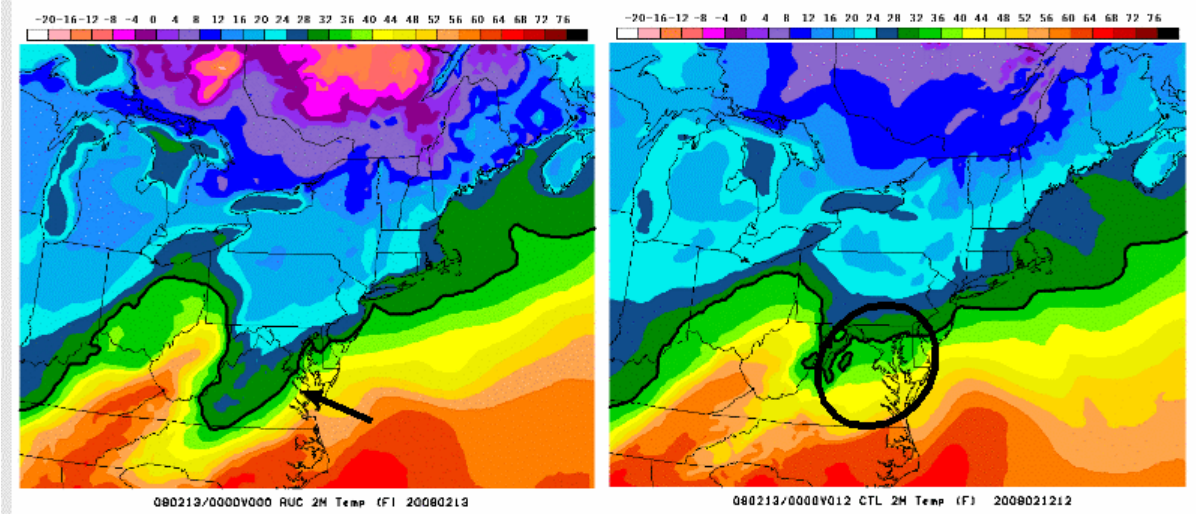

Figure 14: 2-meter temperature (^{o}F) valid 0000 UTC 13 February 2008 from the Rapid Update Cycle analysis (left) and a 21-h forecast from the control WRF-NMM. The 32^{o}F isotherm is highlighted in black.

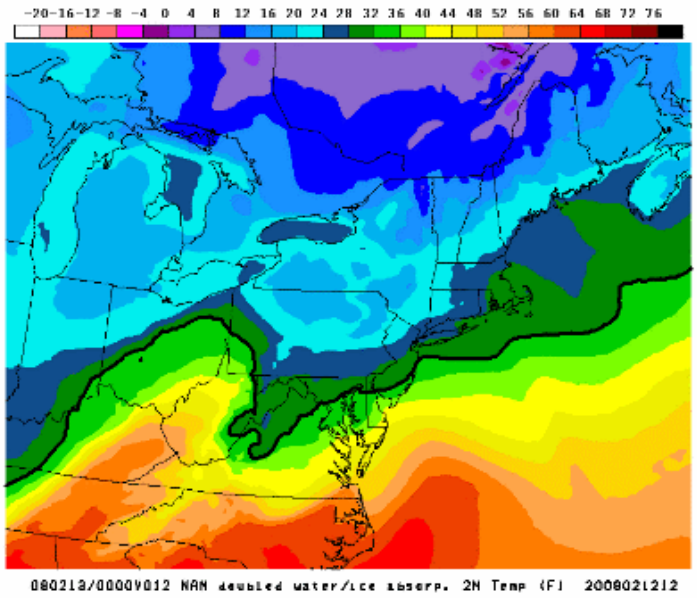

Figure 15: Same as Figure 14, but for a parallel WRF-NMM forecast running with the modification to cloud optical thickness in the December 2008 NAM change package.

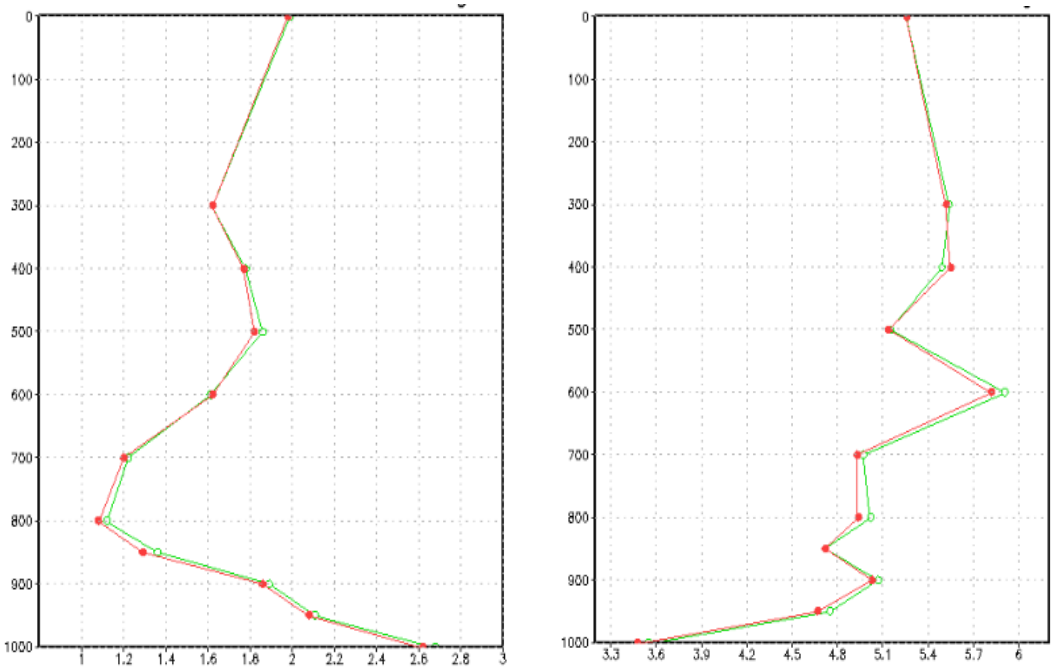

Figure 16: Vertical distribution of the NDAS first guess fit to conventional temperature (left, ^{o}C) and wind (right, ms^{-1}) for the control NDAS (green) and parallel NDAS (red) assimilating TAMDAR/AMDAR aircraft data.

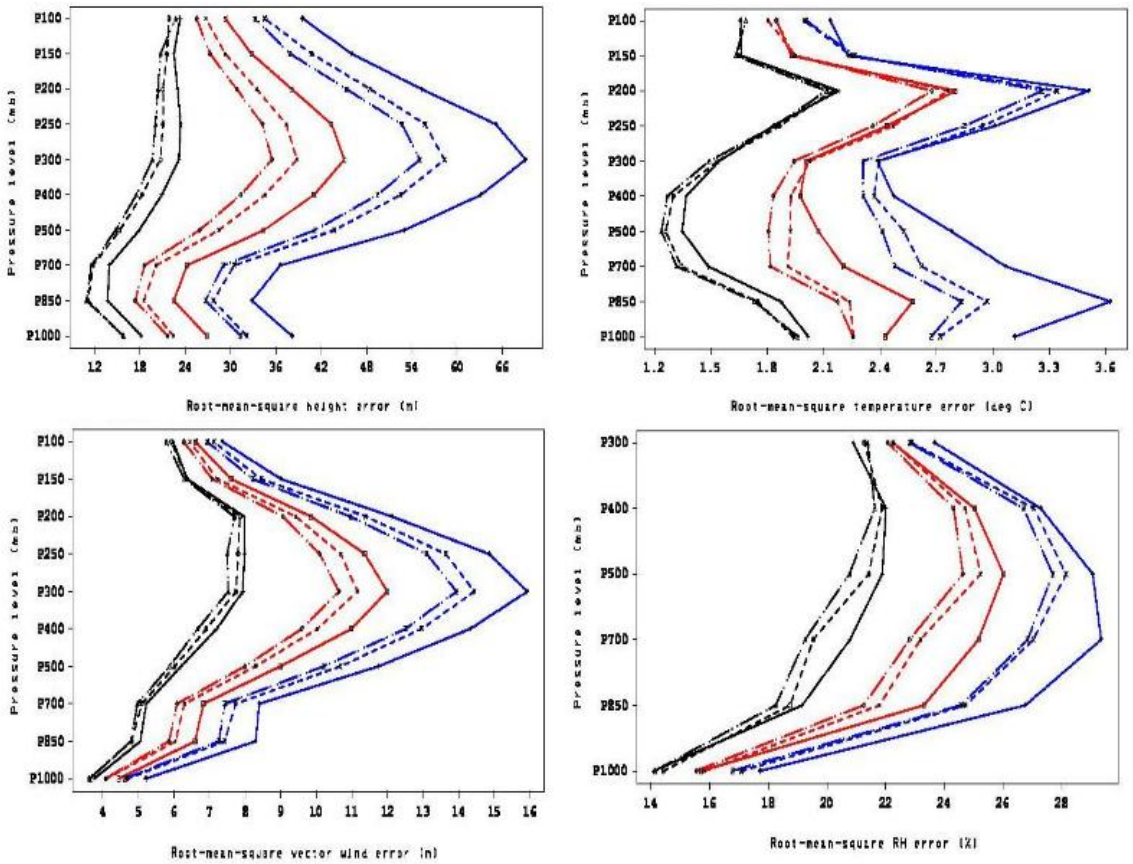

Figure 17: Operational NAM (solid), parallel NAM w/March 2008 changes (dashed), and parallel NAM w/March 2008 changes and partial NDAS cycling (dash-dot) cumulative RMS 24-h (black), 48-h (red) and 72-h (blue) forecast errors versus rawinsondes over the CONUS for height (m, top left), temperature (^{o}C, top right), vector wind (ms^{-1}, bottom left) and relative humidity (%, bottom right) for 17 December 2007 – 25 February 2008.

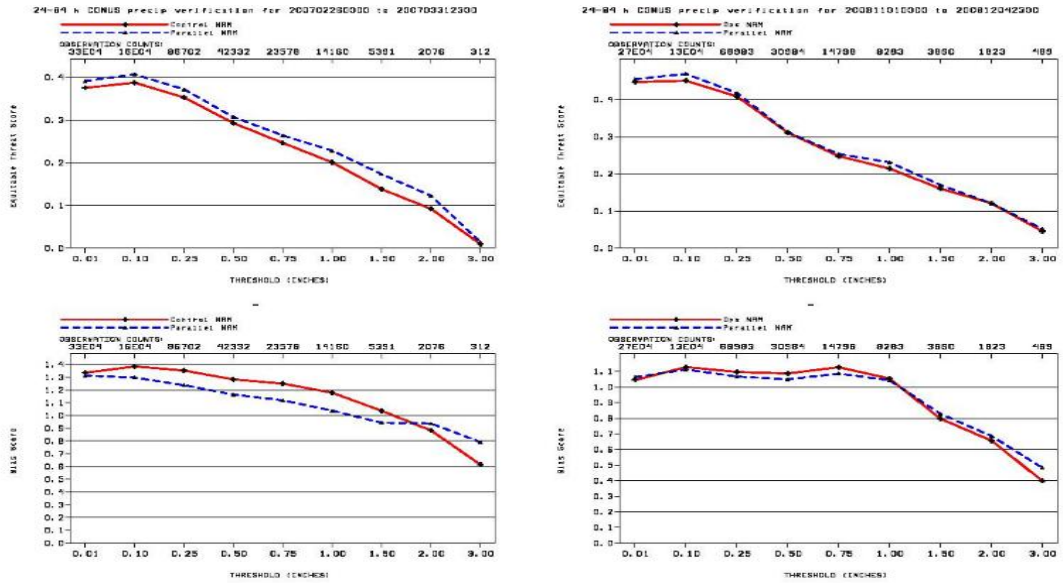

Figure 18: 24-h QPF equitable threat scores (top) and bias scores (bottom) for the December 2008 NAM change package. Left: Control (solid red) and parallel NAM (dashed blue) for March 2007. Right: Operational (solid red) and parallel NAM (dashed blue) from 1 November 2008 – 4 December 2008.

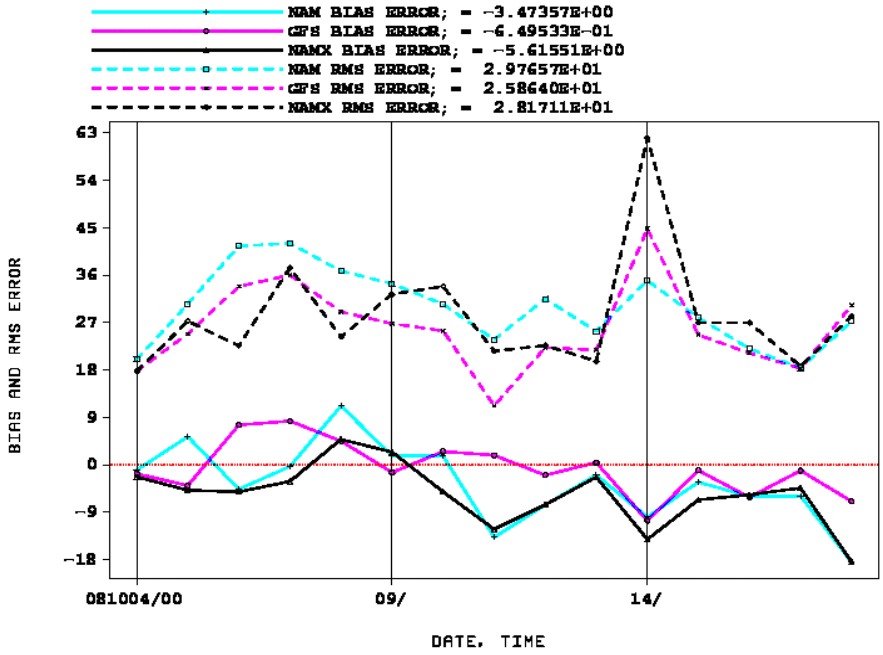

Figure 19: Time series from 4-18 October 2008 of 72-h forecast (valid 0000 UTC) 500 hPa RMS height error (dashed) and height bias error (solid) for the operational NAM (cyan), GFS (magenta), and parallel NAM (black). Average errors for each model for the two week period are at the top of the figure.

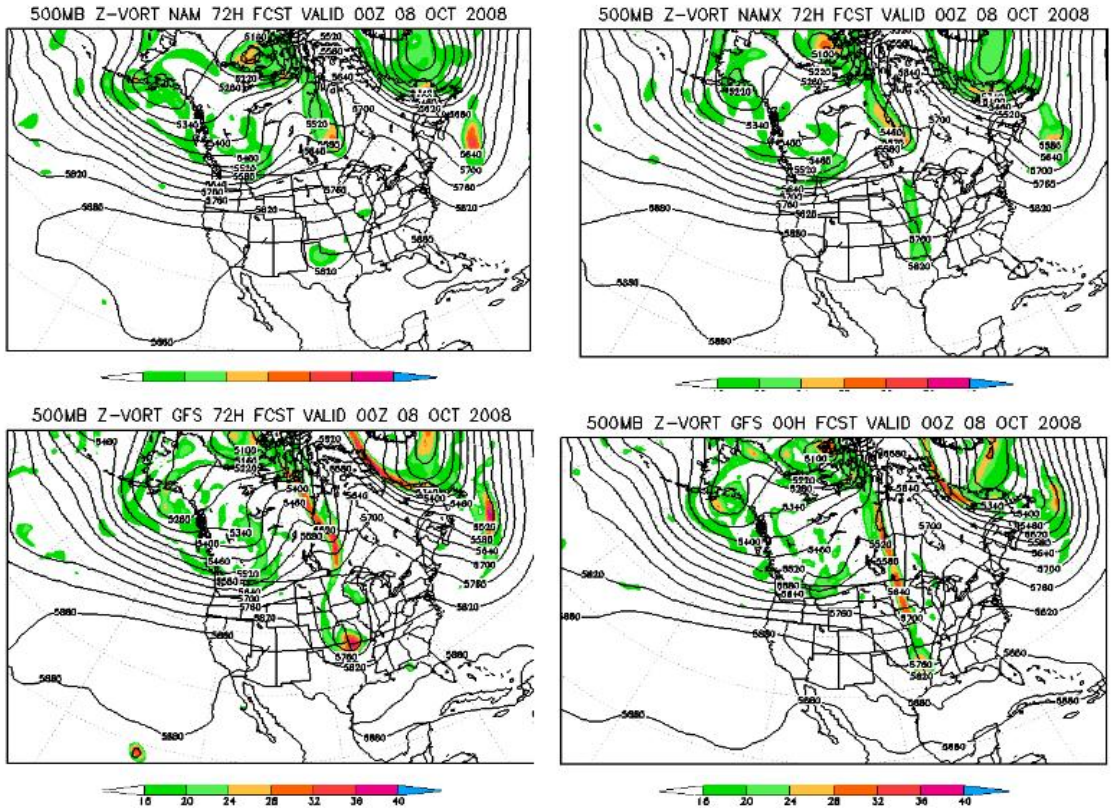

Figure 20: Same as Figure 11, but for 72-h forecasts and GFS analysis valid 0000 UTC 8 October 2008.

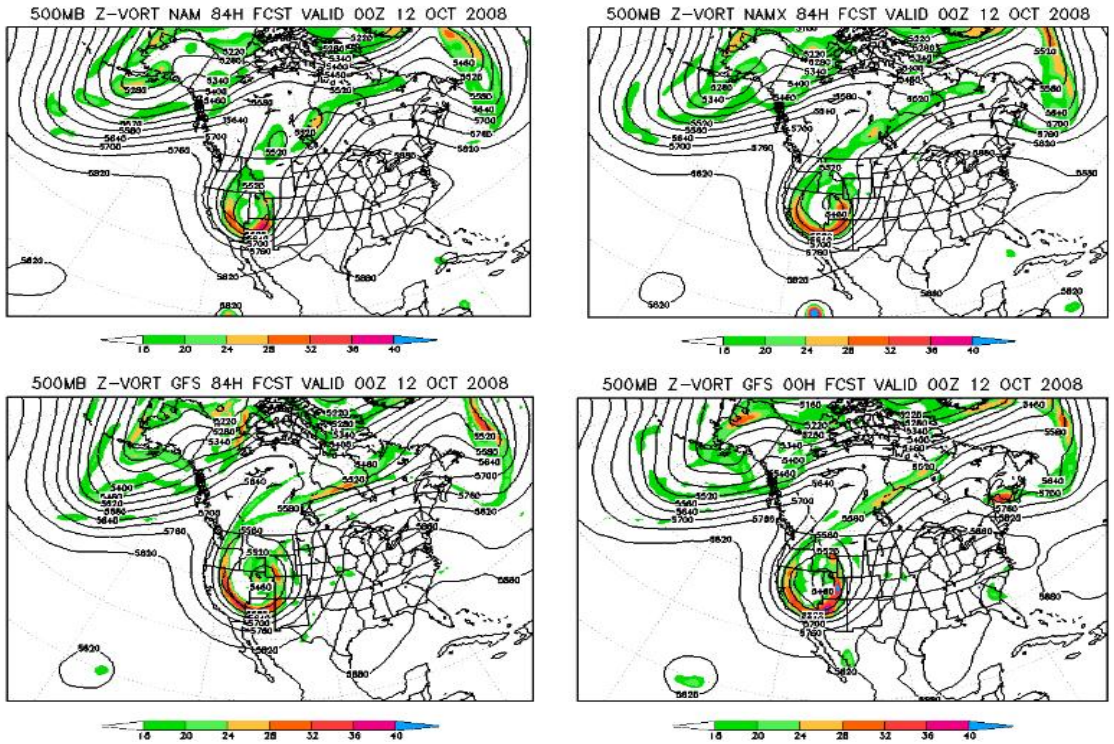

Figure 21: same as Figure 11, but for 84-h forecasts and GFS analysis valid 0000 UTC 12 October 2008.

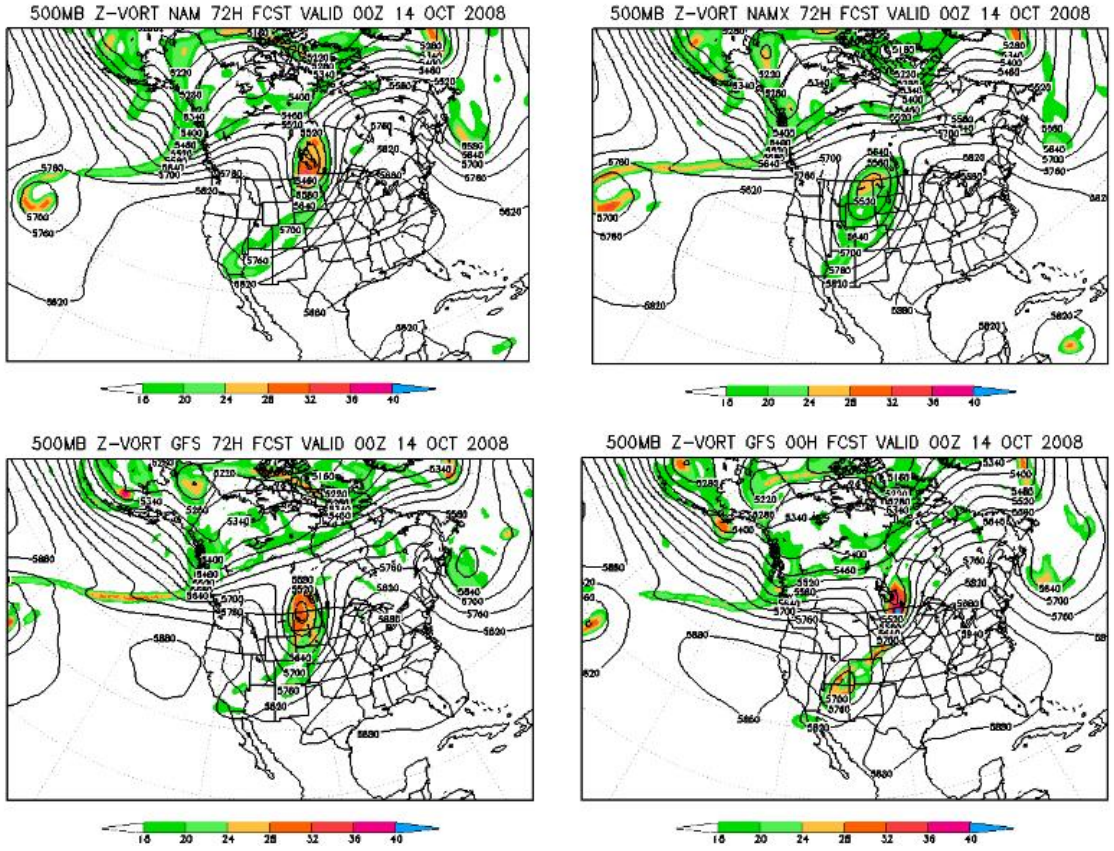

Figure 22: Same as Figure 11, but for 72-h forecasts and GFS analysis valid 0000 UTC 14 October 2008.

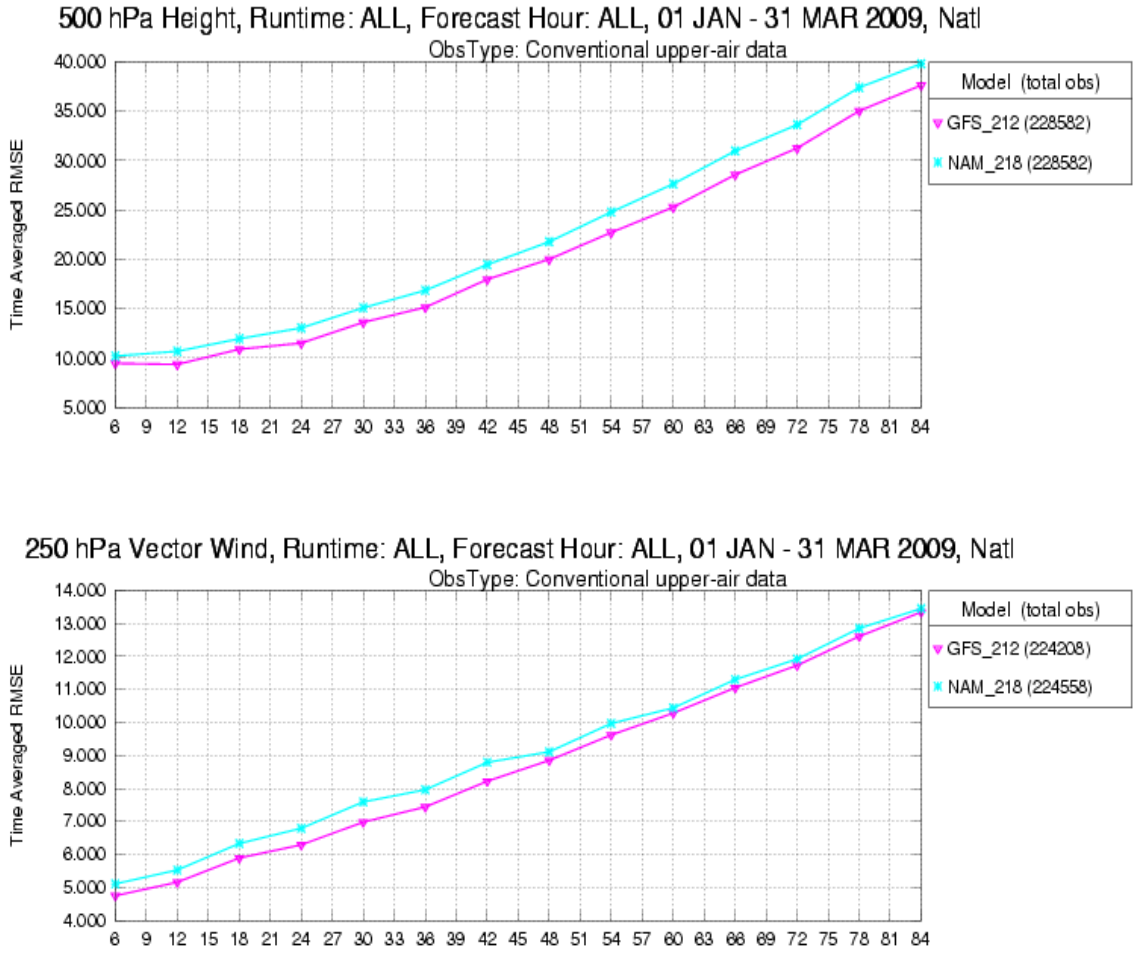

Figure 23: Same as Figure 2, but for January-March 2009.